Contents lists available at ScienceDirect

Comptes Rendus Physique

www.sciencedirect.com

Few body problem / Problème à petit nombre de corps

The Efimov effect in lithium 6

L'effet d'Efimov dans le lithium 6

Pascal Naidon [a,b,*], Masahito Ueda [a,b]

[a] *ERATO Macroscopic Quantum Project, JST, Tokyo 113-0033, Japan*
[b] *Department of Physics, University of Tokyo, 7-3-1 Hongo, Bunkyo-ku, Tokyo 113-0033, Japan*

A R T I C L E I N F O

A B S T R A C T

We analyse the recent experiments investigating the low-energy physics of three lithium 6 atoms in three different internal states with resonant two-body scattering lengths. All observed features are qualitatively consistent with the expected Efimov effect, i.e. the effective universal three-body attraction that arises for large values of the scattering lengths. However, we find that a quantitative description at negative energy requires non-universal two- and three-body corrections due to presently unknown behaviour at short distance. An attempt to implement these corrections is made through energy-dependent parameters that are fitted to the experimental data.

© 2010 Académie des sciences. Published by Elsevier Masson SAS. All rights reserved.

R É S U M É

Nous analysons les récentes expériences concernant la physique à basse énergie de trois atomes de lithium 6 dans des états internes différents avec des longueurs de diffusion résonantes. Toutes les observations s'expliquent qualitativement par l'effet d'Efimov, c'est-à-dire l'attraction universelle effective à trois corps qui survient aux grandes valeurs des longueurs de diffusion. En revanche, il apparaît qu'une compréhension quantitative nécessite des corrections non-universelles à deux et trois corps provenant du comportement inconnu à courte distance. Nous proposons d'implémenter ces corrections par le biais de paramètres dépendant de l'énergie et ajustés à l'expérience.

© 2010 Académie des sciences. Published by Elsevier Masson SAS. All rights reserved.

1. Introduction

In 1970, Vitaly Efimov predicted a peculiar effect [1], a universal effective attraction occurring between three quantum particles with short-range interactions, whenever the two-body interactions are resonant, that is to say their respective two-body scattering lengths are much larger than the typical short range of those interactions. Interestingly, this attraction can bind the three particles to form trimers irrespective of the sign of the scattering lengths, i.e. whether the two-body interaction supports a two-body bound state of similar energy or not. In particular, there is a domain of low energies and large scattering lengths where the three-body physics is dominated by the Efimov attraction. Because this attraction scales as the inverse square of the mean distance between the three particles, as does the kinetic energy, the physics in that region is invariant under discrete scale transformations. As a result, for an infinite scattering length, an infinite set of

---

* Corresponding author at: Department of Physics, University of Tokyo, 7-3-1 Hongo, Bunkyo-ku, Tokyo 113-0033, Japan.
  E-mail address: pascal@cat.phys.s.u-tokyo.ac.jp (P. Naidon).

trimers accumulate at zero-energy, and all these trimers in that region have the same structure described by only a few parameters. For this reason, it is referred to as the (three-body) universal region [2].

Within the last year, the Efimov effect has received a wealth of experimental confirmations from the ultracold atom community, for several kinds of atomic species [3–9]. Evidence of Efimov trimer states appeared as strong enhancement of inelastic collisions due to the presence of an Efimov trimer just below the collisional threshold. These successes were made possible thanks to the existence of magnetic-field induced Fano–Feshbach resonances [10], which enable experimentalists to adjust the two-body scattering length to very large values. The case of lithium 6 atoms [3,6,7,12,13] is particularly striking for several reasons. First of all, unlike the species used in other experiments, lithium 6 atoms are fermions. Since the Efimov attraction does not occur for identical fermions because of the Pauli exclusion principle, they have to be prepared in three distinguishable states 1, 2 and 3. As a result, unlike identical bosons, this system is described by three different scattering lengths, and features three dimers with different binding energies. Fortunately there exists a Feshbach resonance for each pair in the same range of magnetic field, enabling one to have large scattering lengths for all pairs at the same time and the Efimov effect to manifest itself in various ways [11]. In that region, the atoms can pair to form three different kinds of dimers (12), (23), and (31). This creates the possibility of chemical exchange reactions in the universal region, such as $(12) + 3 \rightarrow (13) + 2$ where the energies intersect [14]. Finally, because those dimers are comparatively stable, it is possible to study the connection between dimers and trimers at negative energy. The three-component lithium 6 gas is the first system where a dimer and an atom could be associated into one of the trimers, enabling direct trimer spectroscopy [15].

In this article, we examine in detail how to theoretically reproduce the experimental observations of the Efimov effect in lithium 6. First, we describe the two-body physics, explaining how to model the Feshbach resonance occurring for each pair of atoms. Then, we explain how to deal with the three-body problem, making use of some approximations. We finally apply these models to analyse the experimental observations.

2. Two-body physics: the Feshbach resonances

A lithium 6 atom has a nuclear spin $i = 1$ and a valence electron spin $s = 1/2$, and their coupling leads to 6 different hyperfine states in the electronic ground state. These states can be separated by applying a magnetic field, using the Zeeman effect. They are labelled from 1 to 6 in order of increasing energy $E_{i=1,\ldots,6}$. Since lithium 6 atoms are fermions, we consider all the possible antisymmetrised pairs $\{i, j\}$ of these states as a basis of diatomic channels. The interaction between two atoms A and B depends on the arrangement of the total electronic spin $\vec{S} = \vec{s}_A + \vec{s}_B$ into singlet ($S = 0$) or triplet ($S = 1$) states. It can be written as:

$$\hat{V}(r) = V_0(r)\hat{P}_0 + V_1(r)\hat{P}_1 \tag{1}$$

where r is the distance between the two atoms, $\hat{P}_{S=0,1}$ are the projectors onto the singlet and triplet states, and $V_{S=0,1}(r)$ are the respective singlet and triplet potentials. Because the interaction is non-diagonal in the diatomic channel basis, it leads to a set of coupled Schrödinger equations describing the relative motion of a pair of atoms. As a result, a bare scattering state in one channel can be coupled to a bare bound state in another channel. Since these states have different magnetic moments, it is possible to change their energy difference by applying an external magnetic field. As these states get closer in energy, the scattering length of the dressed states (solution of the full equations including the coupling) becomes larger. At some point, it diverges and changes sign. That phenomenon is a so-called Fano–Feshbach resonance [10]. Thanks to the existence of such resonances, it is possible to make the scattering lengths very large by controlling the magnetic field.

To quantify the effects of the resonances used in the lithium 6 experiments, we solved the coupled-channel equations using singlet and triplet potentials for lithium. The potentials were obtained from the combination of ab-initio calculations and adjustments to previous experimental data from Ref. [16], and are currently the most accurate potentials for lithium 6. They were kindly provided to us by Paul S. Julienne and Eite Tiesinga. From the solutions, we extract important quantities characterising the interaction. For scattering states of an atom pair $\{i, j\}$ at some positive energy $E = \frac{\hbar^2}{m}p^2$ (m is the mass of lithium 6) just above the channel threshold $E_i + E_j$, the component in the channel $\{i, j\}$ (the so-called *open channel*) has the following asymptotic form

$$\psi_{ij}^E(\vec{r}) \propto \frac{\sin pr}{pr} - a_{ij}(p)\frac{\cos pr}{r} \tag{2}$$

which defines the energy-dependent scattering length $a_{ij}(p)$. This quantity is directly related to the more familiar scattering amplitude $f_{ij}(p) = -1/(ip + 1/a_{ij}(p))$. Similarly, for states of negative energy $E = -\frac{\hbar^2}{m}\kappa^2$ below the channel threshold (physical bound states as well as unphysical states), the asymptotic form becomes

$$\psi_{ij}^E(\vec{r}) \propto \frac{\sinh \kappa r}{\kappa r} - a_{ij}(i\kappa)\frac{\cosh \kappa r}{r} \tag{3}$$

which extends the definition of $a_{ij}(p)$ to negative energy. The only physical states are the bound states which decay exponentially at large distance. Therefore they must satisfy the condition

$$a_{ij}(i\kappa) = 1/\kappa$$

whose solutions κ_{ij} correspond to the discrete spectrum of binding energies $E_{ij} = \frac{\hbar^2 \kappa_{ij}^2}{m}$.
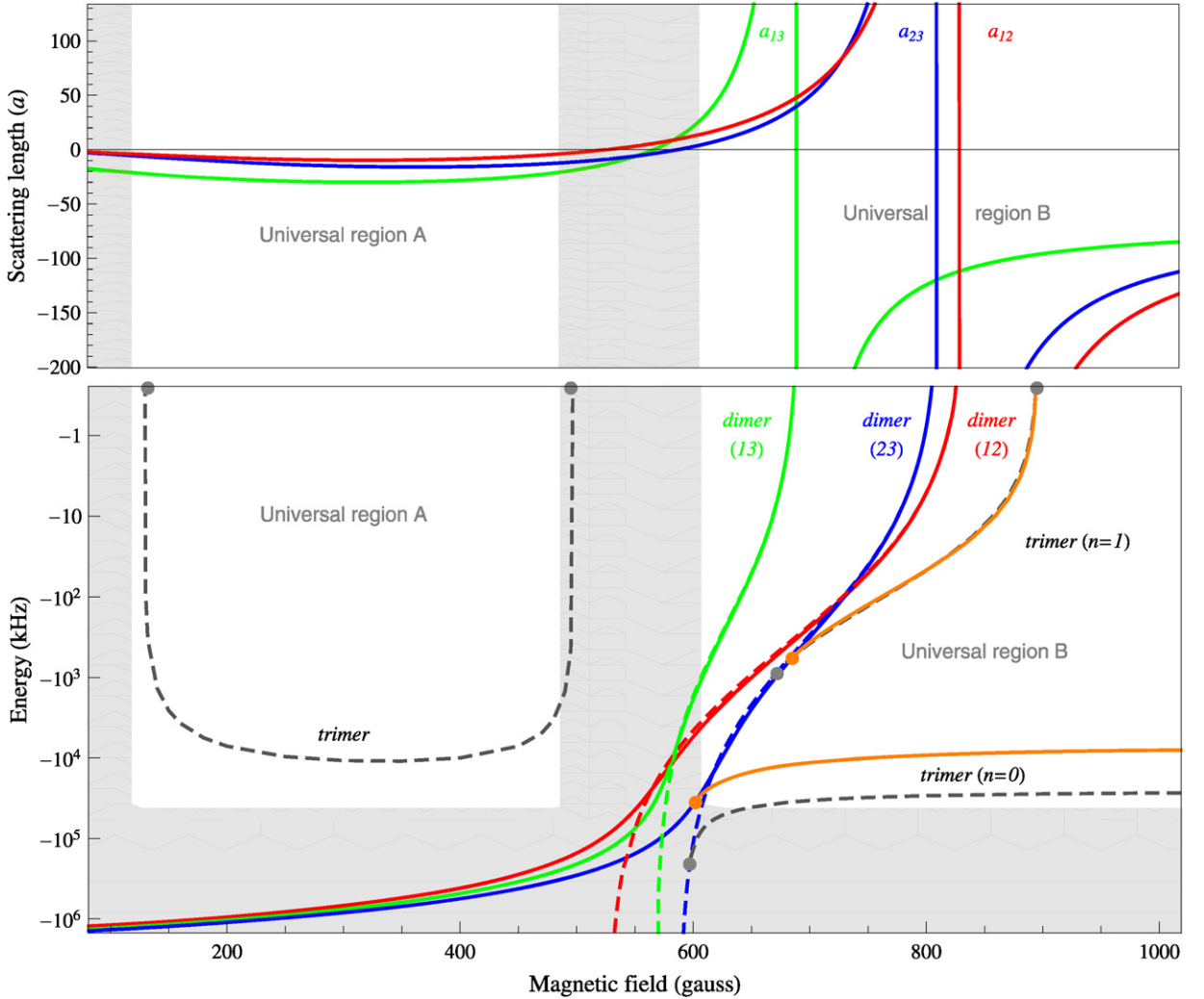
Fig. 1. Top panel: scattering lengths for each pair of atoms as a function of magnetic field. Bottom panel: two-body and three-body energy spectra, as a function of magnetic field. The solid coloured curves correspond to the dimers' energies, and the dashed coloured curves are their universal limit $-\hbar^2/ma_{ij}^2$. The dashed grey curves correspond to the trimers' energies based on the universal theory (with $|\Lambda| = 1.165\bar{a}^{-1}$). The orange curves correspond to the single-channel contact model with both two-body and three-body non-universal corrections implemented through an energy dependence of a_{ij} and Λ. The white areas are the universal regions where all scattering lengths are larger than $3\bar{a}$ and all energies are smaller than $\hbar^2/m(3\bar{a})^2$.

At low energy, the energy-dependent scattering length can be expanded as

$$\frac{1}{a_{ij}(p)} = \frac{1}{a_{ij}} - \frac{1}{2}r_{e,ij}p^2 + \cdots \tag{4}$$

from which we can extract the zero-energy scattering length a_{ij} and the effective range $r_{e,ij}$. Note that bound states with small binding energies must satisfy the universal two-body property $\kappa_{ij} \sim 1/a_{ij}$.

The various scattering lengths, effective ranges and binding energies of the last diatomic bound states are represented in Figs. 1 and 2 as a function of magnetic field for the different atom pairs $\{1,2\}$, $\{2,3\}$, and $\{1,3\}$ relevant to the experiments. According to the universal two-body property $\kappa_{ij} \sim 1/a_{ij}$, a bound state appears at each resonance point where the scattering length a_{ij} becomes infinite, and its binding energy increases as $\hbar^2/ma_{ij}^2$ on the side of positive values of the scattering length. This universal binding energy, only valid for large positive scattering lengths, has been represented as dashed lines in Fig. 1. By comparing the scattering lengths to the typical range of the potentials, the van der Waals length $\bar{a}$ [10], and the binding energies to the van der Waals energy $\hbar^2/m\bar{a}^2$, we can define two different universal regions A and B, which are indicated in Fig. 1. For lithium 6, $\bar{a} \approx 1.5815$ nm.

For convenience, in the rest of the article we will note a_{jk}, κ_{jk}, E_{jk}, etc., as a_i, κ_i, E_i where $\{i,j,k\} = \{1,2,3\}$.
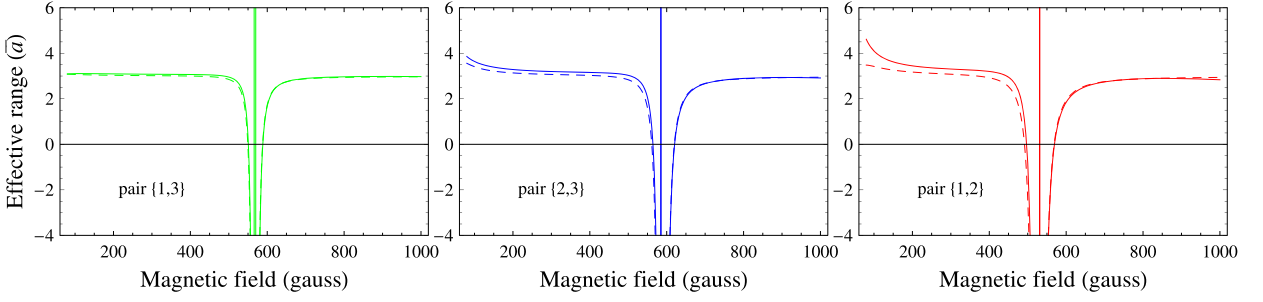
Fig. 2. Effective range of the interaction for each pair of atoms, as a function of magnetic field. Solid curves are calculated from our multichannel two-body model. Dashed curves are obtained from two-channel model in Eq. (16).

3. Three-body physics: approximation schemes

It would be rather difficult to solve the problem of three atoms using the two-body coupled potentials described in the previous section. Moreover, on top of these two-body interactions, there is also a three-body interaction which is presently unknown. However, since we are considering the low-energy properties of the system, a precise knowledge of those interactions and an exact solution of the three-body problem is not necessary. At low energy, the wave function has a large de Broglie wavelength and is affected by the small-scale details of the interactions only through some phase shifts which can be set by choosing appropriate boundary conditions at short distance [1]. Alternatively, one may replace the interactions by pseudopotentials with the same low-energy effects (causing the same phase shifts), or construct a low-energy effective field theory [17] with a few parameters (corresponding again to these phase shifts). All these approaches are essentially equivalent, and are intended to simplify the problem by reducing the number of coordinates, and invoking just a few parameters instead of the complicated knowledge of the two- and three-body interactions. Here we will use the pseudopotential method. We will consider two different pseudopotentials: a single-channel contact pseudopotential, and a two-channel separable pseudopotential of finite range.

3.1. Single-channel contact pseudopotential

Let us start by considering a single-channel pseudopotential as a substitute for the real interaction. The asymptotic behaviour of the two-body scattering state in the open channel in Eqs. (2) and (3) can be reproduced by considering a non-interacting wave ψ with energy $\frac{\hbar^2 p^2}{m}$ and imposing the Bethe–Peierls boundary condition $\psi \propto_{r \to 0} \frac{1}{r} - \frac{1}{a(p)}$, or equivalently $(r\psi(r))'/(r\psi(r)) \to_{r \to 0} -1/a(p)$ which fixes the logarithmic derivative of ψ at short distance r. This condition is equivalent to a Fermi–Huang–Yang contact pseudopotential $\hat{V}$ defined by:

$$\langle \vec{r} | \hat{V} | \psi \rangle = \frac{4\pi \hbar^2 a(p)}{m} \delta^3(\vec{r}) \frac{\partial}{\partial r} (r\psi(\vec{r})) \quad \text{with } p^2 = \lim_{r \to 0} \frac{-\nabla_r^2 \psi(r)}{\psi(r)} \tag{5}$$

By constructing such a pseudopotential $\hat{V}_i(\vec{r}_i)$ for each pair of atoms $\{jk\}$, the three-body Schrödinger equation reads

$$\left[-\frac{\hbar^2}{m} \left(\frac{3}{4} \nabla_R^2 + \nabla_r^2 \right) - E + \hat{V}_1(\vec{r}_1) + \hat{V}_2(\vec{r}_2) + \hat{V}_3(\vec{r}_3) \right] \Psi(\vec{R}, \vec{r}) = 0 \tag{6}$$

where we have chosen a particular set of Jacobi coordinates $(\vec{R}, \vec{r}) = (\vec{R}_1, \vec{r}_1)$ to represent the relative configuration of three atoms in states 1, 2, and 3 – see Fig. 3. The pseudopotentials ensure that in all three Jacobi coordinate systems, the three-body wavefunction Ψ should locally have the following form [18]:

$$\Psi(\vec{R}_i, \vec{r}_i) \underset{r_i \to 0}{=} \left(\frac{1}{r_i} - \frac{1}{a_i(p_i)} \right) \chi_i(\vec{R}_i) + O(r_i), \quad \text{with } p_i^2 = \lim_{r_i \to 0} \frac{-\nabla_{\vec{r}_i}^2 \Psi}{\Psi} = \frac{mE}{\hbar^2} + \frac{3}{4} \frac{\nabla_{\vec{R}_i}^2 \chi_i(\vec{R}_i)}{\chi_i(\vec{R}_i)} \tag{7}$$

which is consistent with the Bethe–Peierls boundary condition for each pair of atoms. This introduces the three quantities $\chi_i(\vec{R}_i)$. From Eq. (6), we obtain

$$\left(-\frac{3}{4} \nabla_R^2 - \nabla_r^2 - \frac{mE}{\hbar^2} \right) \Psi(\vec{R}, \vec{r}) = 4\pi \sum_{i=1,2,3} \chi_i(\vec{R}_i) \delta^3(\vec{r}_i) \tag{8}$$

The solution of this equation in Fourier space is

$$\tilde{\Psi}(\vec{P}, \vec{p}) = \tilde{\Psi}_0(\vec{P}, \vec{p}) + \frac{4\pi}{\frac{3}{4} P^2 + p^2 - mE/\hbar^2 + i\varepsilon} \sum_{i=1,2,3} \tilde{\chi}_i(\vec{P}_i) \tag{9}$$
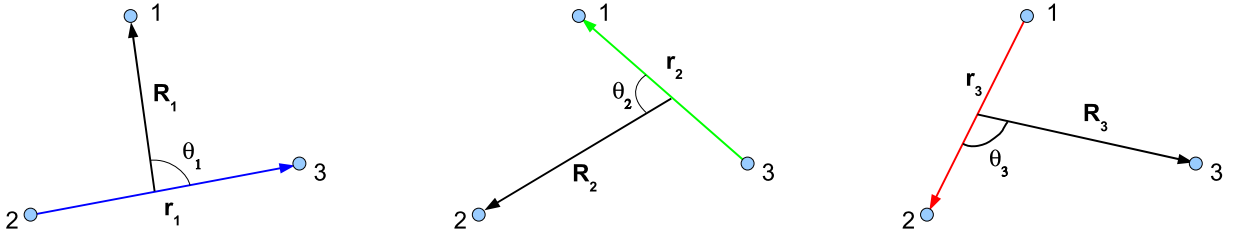
Fig. 3. Jacobi coordinate systems $(\vec{R}_i, \vec{r}_i)$. In Fourier space, we have conjugate wave vectors $(\vec{P}_i, \vec{p}_i)$.

where the term $\tilde{\Psi}_0$ is a solution of the homogeneous (free) three-body equation. It physically corresponds to an incident wave of 3 free atoms $(2\pi)^6 \delta^3(\vec{P} - \vec{P}_0)\delta^3(\vec{p} - \vec{p}_0)$ in the case of positive energy $E = \frac{\hbar^2}{m}(\frac{3}{4}P_0^2 + p_0^2)$, or it must be taken to be zero in the case of states with negative energy E, *i.e.* states Ψ with at least two bound atoms. From Eq. (9) and the definition of χ_i, it follows that the χ_i must satisfy a set of 3 coupled equations known as the Skorniakov–Ter-Martirosian equations [19],

$$\left(\frac{-1}{a_i(i\gamma_P)} + \gamma_P\right)\tilde{\chi}_i(P) - \frac{1}{\pi}\int_0^\Lambda \mathrm{d}q \frac{q}{P} \ln\frac{P^2 + q^2 + Pq - mE/\hbar^2}{P^2 + q^2 - Pq - mE/\hbar^2}\left(\tilde{\chi}_j(q) + \tilde{\chi}_k(q)\right) = \int \frac{\mathrm{d}^3\vec{p}}{(2\pi)^3}\tilde{\Psi}_0(\vec{P}, \vec{p}) \tag{10}$$

with the relative momentum $\gamma_P = \sqrt{\frac{3}{4}P^2 - \frac{mE}{\hbar^2}}$. The derivation is given in Appendix A. If we take the upper bound Λ of the integral in the left-hand side of Eq. (10) to be infinite, the equations admit several solutions, as was noted by G.V. Skorniakov and discussed by G.S. Danilov [20]. This is because the replacement of real interactions by two-body contact interactions is in general not sufficient to have a well-defined three-body problem. In special situations of two-body interactions with a large negative effective range, a unique solution is determined by the equations [18]. Otherwise, an extra boundary condition on the wave function at very short distance where all three atoms are close to one another is necessary. Cutting off the integral at some momentum Λ [21] precisely provides such a condition, as shown in Appendix B.

In his original papers, Vitaly Efimov considered an energy-independent scattering length $a(p) = a$. As we mentioned before, at the two-body level this approximation is valid only in the universal region of large scattering lengths (compared to the range of the interactions). Hence, Eq. (10) with an energy-independent scattering length are equivalent to the *universal theory* originally proposed by Vitaly Efimov to investigate the universal properties of three-body systems with large scattering lengths. Note that the energy-dependence of $a(k)$ brings finite-range corrections to the universal theory, including the effective range correction [22] as can be seen from Eq. (4).

3.2. Coupled-channel separable pseudopotential

Although the previous approach does take into account finite-range corrections, it may still look oversimplified because it neglects the coupled-channel nature of the real atomic interactions near Feshbach resonances. To account for this, one may substitute the real interaction by an effective two-channel interaction $\hat{U}$ that reproduce most features of the original Feshbach resonances [23,24]. It can be written as

$$\hat{U} = \hat{U}_o|o\rangle\langle o| + \hat{U}_c|c\rangle\langle c| + \hat{U}_{oc}|c\rangle\langle o| + \hat{U}_{co}|o\rangle\langle c| \tag{11}$$

where $|o\rangle$ and $|c\rangle$ correspond to open and closed channels, respectively.

Let us first look at two atoms interacting with this effective potential. The two-body Hamiltonian is $\hat{K} + \hat{U}$, where $\hat{K}$ is the relative kinetic energy. To model a resonance with a single bound state ϕ of energy E_b in the closed channel, we take the closed-channel Hamiltonian $\hat{K} + \hat{U}_c$ to be $E_b|\phi\rangle\langle\phi|$ and the channel-coupling term as $\hat{U}_{oc} = \hat{U}_{co}^\dagger = W|\phi\rangle\langle\phi|$. A two-body state $|\psi\rangle$ can be written as a superposition of open and closed-channel components $|\psi\rangle = \int \frac{\mathrm{d}^3\vec{p}}{(2\pi)^3} A(\vec{p})|\vec{p}\rangle|o\rangle + B|\phi\rangle|c\rangle$, where $|\vec{p}\rangle$ is the plane wave for two atoms with relative momentum $\vec{p}$, and the Schrödinger equation $(\hat{K} + \hat{U} - E)|\psi\rangle = 0$ leads to:

$$(E_b - E)B + 2\int \frac{\mathrm{d}^3\vec{q}}{(2\pi)^3}A(\vec{q})W\phi^*(\vec{q}) = 0 \tag{12}$$

$$\left(\frac{\hbar^2 k^2}{m} - E\right)A(\vec{p}) + \int \frac{\mathrm{d}^3\vec{q}}{(2\pi)^3}A(\vec{q})U_o(\vec{q}, \vec{p}) + BW\phi(\vec{p}) = 0 \tag{13}$$

By assuming that the open-channel potential is separable [23–26], $U_o(\vec{q}, \vec{p}) = \frac{4\pi\hbar^2}{m}\lambda\phi^*(\vec{q})\phi(\vec{p})$, we can group the last two terms in the second equation, which greatly simplifies the problem. This arbitrary choice is permitted since the small-scale details of the interaction are unimportant as long as they correctly reproduce the low-energy physics, as argued before. For

the same reason, we can arbitrarily choose the functional form of $\phi(p)$. Following [23,24], we choose for convenience a Gaussian form $\phi(p) = e^{-\frac{1}{2}(bp)^2}$ with range b.

Eliminating B in Eq. (13) and solving at positive energy $E = \frac{\hbar^2 p_0^2}{m}$, one obtains:

$$A(\vec{p}) = A_0(\vec{p}) - \frac{T(p_0, p)}{\frac{\hbar^2 p^2}{m} - E - i\varepsilon} \tag{14}$$

where $A_0(\vec{p}) = (2\pi)^3 \delta^3(\vec{p} - \vec{p}_0)$ corresponds to an incident plane wave of momentum $\vec{p}_0$, and we introduced the two-body T-matrix element

$$T(p_0, p) = \left(\frac{4\pi\hbar^2}{m} \lambda - \frac{2|\Lambda|^2}{E_b - E} \right) \left(\int \frac{d^3\vec{q}}{(2\pi)^3} \phi^*(q) A(q) \right) \phi(p) \tag{15}$$

Solving for $T(p_0, p)$ self-consistently using the last two formulæ, we deduce that the scattering length $a(p) = -[(\frac{m}{4\pi\hbar^2} T(p, p))^{-1} + ip]^{-1}$ takes the form [26]

$$a(p) = \left\{ \left[\left(\lambda - \frac{\alpha}{E_b - E} \right)^{-1} + \frac{1}{\sqrt{\pi}b} \right] e^{(pb)^2} + p\,\mathrm{Erfi}(pb) \right\}^{-1} \tag{16}$$

where $\alpha = \frac{m}{2\pi\hbar^2}|\Lambda|^2$, and Erfi is a real function related to the standard error function Erf by $\mathrm{Erfi}(z) = \mathrm{Erf}(iz)/i$. By adjusting the parameters λ, α, E_b and b, we can construct for each pair of atoms $\{j, k\}$ a pseudopotential $\hat{U}_i$ which reproduces the energy-dependent scattering length $a_i(p)$ of the real interaction.

We now consider three atoms 1, 2, 3 interacting through these pseudopotentials $\hat{U}_1$, $\hat{U}_2$ and $\hat{U}_3$. The three-body wave function can be written as:

$$|\Psi\rangle = \int \frac{d^3\vec{P}}{(2\pi)^3} \frac{d^3\vec{p}}{(2\pi)^3} A(\vec{P}, \vec{p}) |\vec{P}\rangle_1 |\vec{p}\rangle_{23} + \sum_{(i,j,k)=(1,2,3)} \int \frac{d^3\vec{P}}{(2\pi)^3} B_i(\vec{P}) |\vec{P}\rangle_i |\phi\rangle_{jk} \tag{17}$$

where $|\vec{P}\rangle_i$ is the plane wave with momentum $\vec{P}$ for the relative motion between atom i and the centre of mass of the pair of atoms j and k, $|\vec{p}\rangle_{jk}$ is the plane wave of momentum $\vec{p}$ for the relative motion between atoms j and k, and $|\phi\rangle_{jk}$ is the closed-channel bound state for the pair of atoms j and k. Defining the quantity

$$\tilde{\beta}_i(q) = -\left(\lambda_i - \frac{\Lambda_i}{E_i + \frac{3}{4}\frac{\hbar^2 Q_k^2}{m} - E + i\varepsilon} \right) \int \frac{d^3\vec{p}}{(2\pi)^3} \phi^*(p_i) A(Q_i, p_i) \tag{18}$$

we obtain an equation similar to Eq. (9) for the open-channel component A,

$$A(\vec{P}, \vec{p}) = A_0(\vec{P}, \vec{p}) + \frac{4\pi}{\frac{3}{4}P^2 + p^2 - mE/\hbar^2 + i\varepsilon} \sum_{i=1,2,3} \tilde{\beta}_i(\vec{P}_i) \phi(\vec{p}_i) \tag{19}$$

where A_0 is an incident plane wave $(2\pi)^6 \delta^3(\vec{P} - \vec{P}_0) \delta^3(\vec{p} - \vec{p}_0)$ for positive energy $E = \frac{\hbar^2}{m}(\frac{3}{4}P_0^2 + p_0^2)$, or zero for negative energy. The $\tilde{\beta}_i$ then satisfy the generalised Skorniakov–Ter-Martirosian coupled equations,

$$|\phi(i\gamma_P)|^2 \left(\frac{-1}{a_i(i\gamma_P)} + \gamma_P \right) \tilde{\beta}_i(P) - \frac{1}{\pi} \int_0^\Lambda q^2\,dq \int_{-1}^1 du\, \frac{\phi^*\left(\sqrt{q^2 + \frac{P^2}{4} + Pqu}\right)\phi\left(\sqrt{\frac{q^2}{4} + P^2 + Pqu}\right)}{P^2 + q^2 - Pq - mE/\hbar^2} \left(\tilde{\beta}_j(q) + \tilde{\beta}_k(q) \right)$$

$$= \int \frac{d^3\vec{p}}{(2\pi)^3} \phi^*(\vec{p}) A_0(\vec{P}, \vec{p}) \tag{20}$$

Note that these equations are very similar to Eq. (10). In particular, all the two-body physics is contained in the energy-dependent scattering length a_i, except for the terms ϕ. When $\phi \to 1$, *i.e.* when the range b of the interaction goes to zero, we formally retrieve the single-channel contact interaction equations (10). This indicates that apart from the terms ϕ there is little difference between the two approaches. Here, the presence of ϕ with non-zero range b effectively cuts off the integral at high momenta, so that we can safely take $\Lambda \to \infty$. In fact, the range b of the pseudopotential plays the role of Λ in Eq. (10), *i.e.* it characterises the three-body behaviour at short distance.

It might seem unreasonable to choose b, which is determined by the two-body interaction only, in order to characterise a three-body property. In general, the short-range three-body behaviour should also depend on a three-body interaction between the atoms. To be consistent, a three-body interaction should be added in the problem. Another approach, taken in Ref. [24], is to regard b not as a parameter describing the real two-body interaction (for example its effective range), but as a free two-body parameter that is adjusted to set the combined effects of the real two-body and three-body interactions.

3.3. Models

To analyse the experimental results, we will consider three different three-body models:

- The *universal model* is given by Eq. (10) with energy-independent scattering lengths a_i that are obtained from the two-body calculation of Section 1, and Λ is a free parameter.
- The *single-channel contact model* is given by Eq. (10) with energy-dependent scattering lengths $a_i(p)$ given by Eq. (16), where we set the parameters λ_i α_i, $E_{b,i}$, and b so as to reproduce the two-body quantities calculated in Section 1, namely a_i, $r_{e,i}$ and κ_i, as a function of magnetic field. The reason why we use this two-body model instead of the real $a_i(p)$ is that it is numerically intractable to calculate the real $a_i(p)$ at negative energy due to the divergence of sinh and cosh at large distance in Eq. (3). Nevertheless, this simple two-channel model should be very close to the real $a_i(p)$ in the low-energy domain that we are interested in.
- The *two-channel separable model* is given by Eq. (20) with the scattering lengths $a_i(p)$ given again by Eq. (16).

4. Analysis of the experiments

There have been two sets of experiments. The first one [3,12,13] consisted in measuring the three-body recombination rate in a gas of atoms equally distributed in the lowest three spin states. Three-body recombination is the process where three colliding atoms recombine to form a combination of states with lower internal energy, such as a deep dimer and a free atom. At the Feshbach resonance locations, the three-body recombination is strongly enhanced by the very large scattering length. Away from these points, other peaks were found and attributed to recombination enhancement by the presence of Efimov trimers at zero energy. Indeed, whenever a trimer state exists just below the collisional threshold of three atoms, the three atoms resonate, which increases their probability to be close together and recombine. In the second set of experiments [6,7], a gas of dimers and atoms was prepared, and inelastic collisions by relaxation to deeper dimer states were observed. The relaxation rate was also found to be enhanced at two magnetic field values due to the presence of two Efimov trimers just below the collision threshold. Recently, one of the two trimers' energy was directly observed by association spectroscopy [15,27]. These experiments thus provided some partial information about the spectrum of Efimov trimers at both zero and negative energies. The general spectrum based on these results is given in Fig. 1.

4.1. Experiments at zero energy (three-body recombination)

When three atoms in different states collide and recombine, the density n_i of atoms in each state i decreases according to the rate equation:

$$\dot{n}_i = -K_{\text{rec}} n_i n_j n_k \tag{21}$$

where K_{rec} is the recombination coefficient. By measuring the variation of the number of atoms, and taking into account other kinds of loss, it is possible to extract the recombination coefficient. The clearest evidence of the enhancement of this coefficient by the presence of an Efimov trimer at zero-energy is the peak found around 895 G by Williams et al. [3]. It is indeed located in a region of very large scattering lengths where the universal theory should be valid

To calculate the recombination coefficient, we proceed as follows. We distinguish between two types of dimers: dimers which are included in the theory (through the solutions of $1/a(i\kappa) = \kappa$), referred to as *shallow dimers*, and dimers which are not included in the theory, referred to as *deep dimers*. Recombination to shallow dimer (jk) appears in the three-body wave function as an outgoing wave between dimer (jk) and atom i. This means that $\tilde{\chi}_i$ or $\tilde{\beta}_i$ can be written as:

$$\tilde{\chi}_i(P) = \sqrt{\mathcal{N}_i} \, \frac{4\pi F_i(P)}{P^2 - Q_i^2 - i\varepsilon}, \qquad \tilde{\beta}_i(P) = \sqrt{\mathcal{N}_i'} \, \frac{4\pi F_i(P)}{P^2 - Q_i^2 - i\varepsilon} \tag{22}$$

where $Q_i = \sqrt{\frac{4}{3}(\frac{m}{\hbar^2}E + \kappa_i^2)}$ is the relative momentum between dimer (jk) and atom i, and $\mathcal{N}_i = (\int \frac{d^3 p}{(2\pi)^3} |\frac{1}{p^2 + \kappa_i^2}|^2)^{-1} = \frac{\kappa_i}{2\pi}$ and $\mathcal{N}_i' = (\int \frac{d^3 p}{(2\pi)^3} |\frac{\phi(p)}{p^2 + \kappa_i^2}|^2)^{-1} \mathcal{P}_o$ are factors ensuring that the dimer wavefunction is properly normalised to unity, or the probability $\mathcal{P}_o$ to be in the open channel, respectively. The recombination coefficient K_{rec}^i to shallow dimers (jk) is then obtained by calculating the flux of that outgoing wave [18,25]:

$$K_{\text{rec}}^i = \frac{3h}{m} Q_i |F_i(Q_i)|^2 \tag{23}$$

Recombination to deep dimers occurs at distances on the order of the deep dimers' size, typically given by the range of the interactions. Therefore, the coefficient for recombination to deep dimers can be estimated by calculating the probability of finding the three atoms within that range [28,29]:

$$K_{\text{rec}}^{(\text{deep})} = \xi \frac{\hbar}{m\mathcal{R}_0^2} \int\limits_{\sqrt{\frac{4}{3}R^2 + r^2} < \mathcal{R}_0} d^3\vec{R}\, d^3\vec{r} \, |\Psi(\vec{R}, \vec{r})|^2 \tag{24}$$
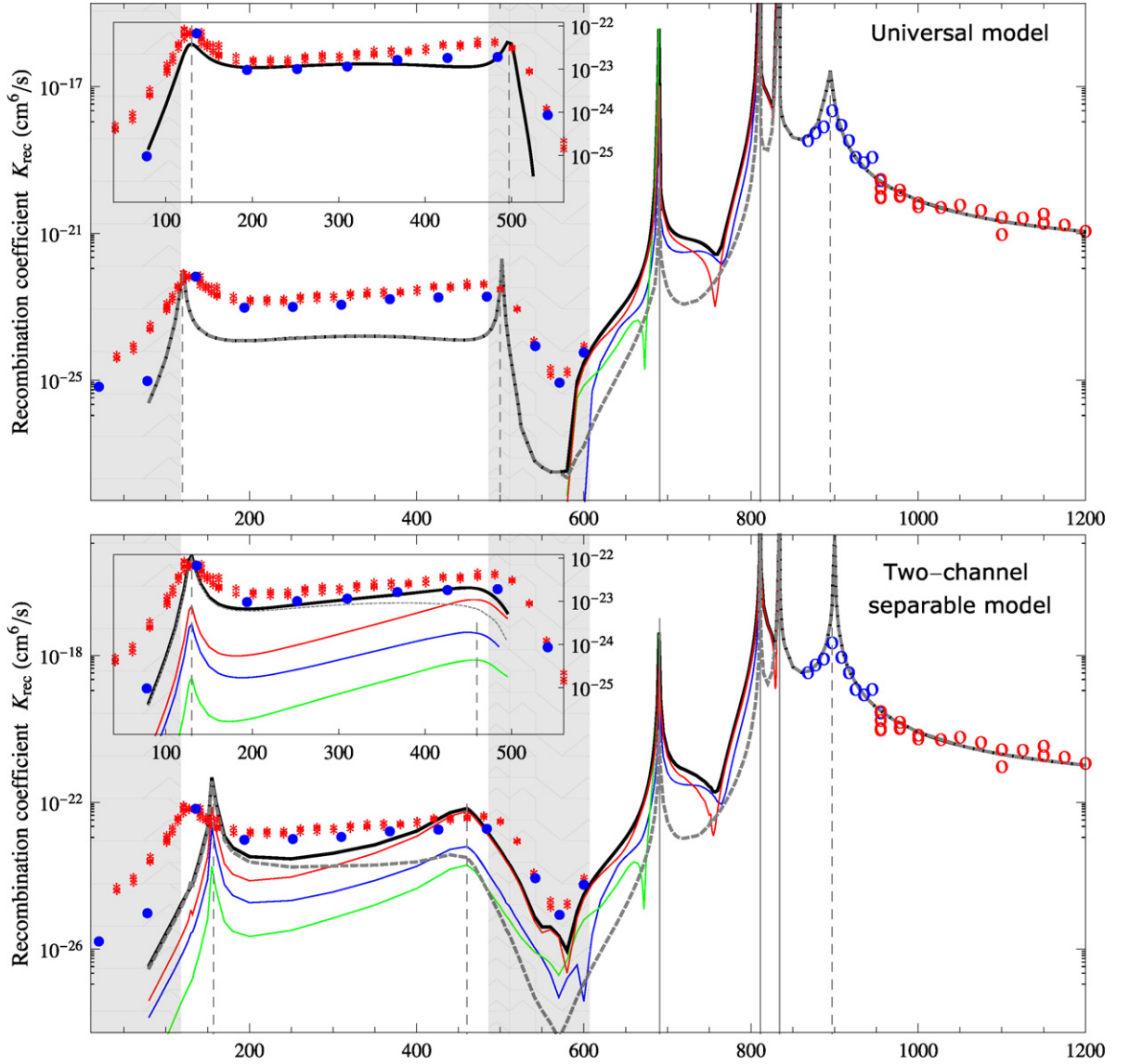
Fig. 4. Recombination coefficient K_{rec} as a function of magnetic field. The stars, dots and circles indicate the experimental measurements of Refs. [12,13], and [3], respectively. Top panel: calculations from the universal model for $|\Lambda| = 1.165\bar{a}^{-1}$ and $\eta = 0.016$. The insert shows results in universal region A for $|\Lambda| = 1.076\bar{a}^{-1}$ and $\eta = 0.115$. Bottom panel: calculations from the two-channel separable model for $b = 1.31\bar{a}$ and $\xi = 0.08$. The insert shows results in universal region A for $b = 0.75\bar{a}$ and $\xi = 0.5$. In both panels, thick black curves show the total recombination coefficient, dashed grey curves show the recombination coefficient to deep dimers, and coloured curves show the recombination to shallow dimers: (13) green, (23) blue, and (12) red.

The results are not very sensitive to the precise choice of the range $\mathcal{R}_0$, and the constant factor ξ is expected to be on the order of unity. Typically, if $\mathcal{R}_0$ varies by 10%, the rate $K_{rec}^{(deep)}$ changes by 6%. As a typical size, we chose $\mathcal{R}_0 = \bar{a}$. The total recombination coefficient is $K_{rec} = \sum_i K_{rec}^i + K_{rec}^{deep}$. Alternatively, in the contact interaction model, one can set a complex three-body parameter $\Lambda = |\Lambda|e^{i\eta}$, where $\eta > 0$ phenomenologically reproduces short-distance losses due to recombination to deep dimers. In that case, the total recombination coefficient at zero energy is given by (see Appendix C)

$$K_{rec} = \frac{4h}{m} \text{Im} \sum_i \tilde{\chi}_i(0) \tag{25}$$

This method also has the advantage of taking into account the broadening effect of the loss strength η on the recombination profile as a function of magnetic field. We checked that the two methods give similar results. The calculated recombination coefficients for different models are represented in Fig. 4.

In the universal model, we have to adjust $|\Lambda|$ to $1.165\bar{a}^{-1}$ and η to 0.016 ($\xi \approx 0.8$) in order to reproduce the 895 G peak. This peaks correspond to the appearance of an Efimov trimer at the three-body collisional threshold (zero energy) as

represented in Fig. 1. Then we obtain the variation of the recombination coefficient around 895 G in the whole universal region B, as first calculated by Eric Braaten et al. [30]. We extend the calculation to low magnetic field in universal region A where earlier measurements of recombination were performed [12,13]. Interestingly, the same three-body parameter roughly reproduces the variation of the recombination coefficient: a plateau with two peaks on both ends. However the two peaks are not exactly at the right locations. This is not unexpected, since different universal regions separated by zero crossings of the scattering lengths are known to have different three-body phases in general [31]. Changing the value of $|\Lambda|$ to $1.076\bar{a}^{-1}$, and η to 0.115 gives a fair agreement between the measured recombination and the universal model – see the insert in the top panel of Fig. 4. Note that the two peaks correspond again to zero-energy crossings of a trimer in Fig. 1. This was in fact the first indication of the underlying Efimov physics in lithium 6 [32–34]. However the calculated recombination coefficient shows two marked peaks, while in the experimental data the left peak is much more pronounced than the right one. Variations of the loss parameter η with magnetic field were subsequently proposed to improve the agreement of the universal model with the data [35,36]. The reason is that in the universal model the least-bound dimers cease to exist at low magnetic field because the scattering length becomes negative. Since in reality those dimers are still present, the loss parameter η effectively accounts for transitions to these dimers. As their energy varies with magnetic field, it was inferred that η should also change with magnetic field [36].

In the single-channel contact model and the two-channel separable model, the least-bound dimers are explicitly included over the full range of magnetic field. For binding energies larger than the typical van der Waals energy associated with the range the interaction, corresponding to magnetic field smaller than 600 G, their description becomes unrealistic. However their energy remains accurate, and they still provide a simple model for the recombination mechanism. In the single-channel contact model, we adjust $|\Lambda|$ to $1.455\bar{a}^{-1}$ and $\eta = 0.0033$ ($\xi \approx 0.8$) to reproduce the 895 G peak. Note that because the scattering lengths are now energy-dependent, the values of $|\Lambda|$ and η have been altered in order to obtain the same physical situation. This is because the choice of the high-energy (*i.e.* short-distance) behaviour of the two-body interactions affects the choice of the three-body phase. The calculated recombination rate in the universal region B is nearly identical to the universal model. It is however numerically difficult to extend the calculation to the universal region A, presumably because in that region the dimers' binding momenta κ_i are close or even exceed the cutoff momentum Λ. This problem does not occur for the two-channel separable model.

In the two-channel separable model, we first adjusted b to $1.31\bar{a}$ to match the effective range of the two-body interaction – see Fig. 2. Surprisingly, this choice perfectly reproduces the location of the peak at 895 G. Again, the results in universal region B are very similar to those of the universal model. In universal region A, however, the results are different and significantly off the observed peak locations. Changing b to $0.75\bar{a}$ (thus using a wrong effective range, while preserving the correct scattering lengths and dimer binding energies) we can effectively change the three-body phase and get better agreement – see bottom panel insert in Fig. 4. These numerical results also seem consistent with the semi-analytical approach of Ref. [36] based on the universal theory and a magnetic-field-dependent η.

From all these results, we conclude that the three-body physics of lithium 6 at zero energy is essentially consistent with the universal theory.

4.2. Experiments at negative energy

From the previous analysis, it is possible to predict the energy spectrum of trimers using the previously adjusted parameters. The spectrum based on the universal model, first predicted in Refs. [30,33,34], is shown in Fig. 1. In universal region A, it predicts a trimer state which connects to no dimer but dissociates into three atoms at two magnetic field values corresponding to the two three-body recombination peaks. In universal region B, it predicts the existence of two trimers which connect to the dimer (23) at 598 G and 672 G. In fact, the first meeting point is outside the universal region where the dimer binding energy clearly deviates from the universal formula $\hbar^2/ma^2$. Therefore, it was expected in Ref. [30] to be unreliable. On the other hand, the 672 G prediction is right in the universal region and was thought to be reliable. It turns out that the dimer energy still has a small but appreciable deviation from universality at that magnetic field, due to two-body finite-range corrections. However, computing the trimer energy with the single-channel contact or two-channel separable model (both of which include those two-body finite range corrections) leads to a similar trimer energy curve which again meets the dimer curve at around 672 G – see Fig. 5. In other words, the two-body finite range corrections shift both the dimer and trimer energies, but do not modify the magnetic field of their meeting point.

4.2.1. Atom–dimer relaxation

To check those predictions, experimentalists prepared a mixture of dimers (23) and atoms 1, and observed the rate of relaxation to deep dimers as atoms and dimers collide. The density n_1 of atoms in state 1 therefore decreases according to the rate equation:

$$\dot{n}_1 = -K_{\text{rel}} n_1 n_{23} \tag{26}$$

where n_{23} is the density of dimers (23) and K_{rel} is the relaxation coefficient. Calculating the relaxation coefficient from the theory is similar to the case of the recombination coefficient. For the case of dimer (23) colliding with atom 1 at energy
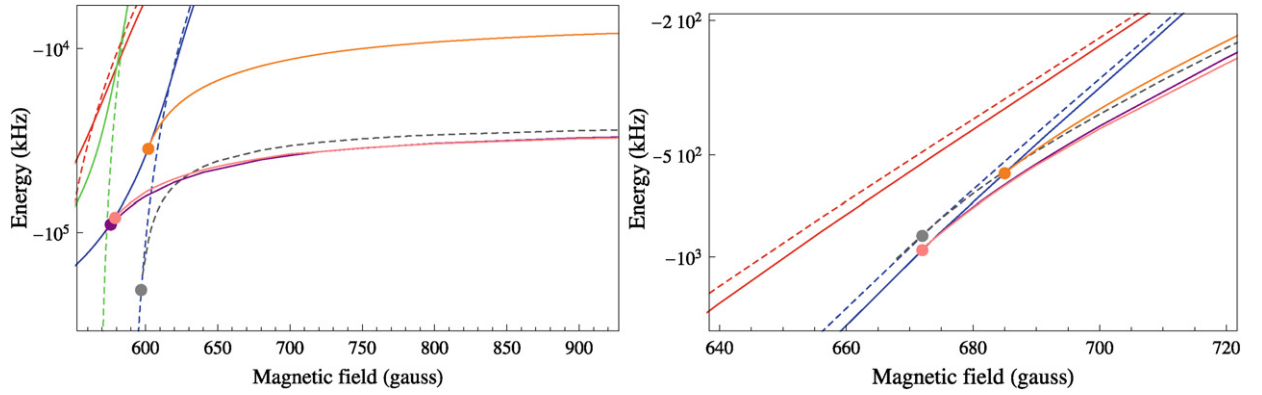
Fig. 5. Trimers and dimers connection regions. Left: ground-state Efimov trimer. Right: first excited-state Efimov trimer. Dimer curves are the same as in Fig. 1. Trimer curves are obtained for different models: universal model (dashed grey), single-channel contact model (purple), two-channel separable model (pink), and single-channel model with the energy-dependent parameter Λ given in Fig. 8 (orange). All models feature a zero-energy resonance at 895 G.
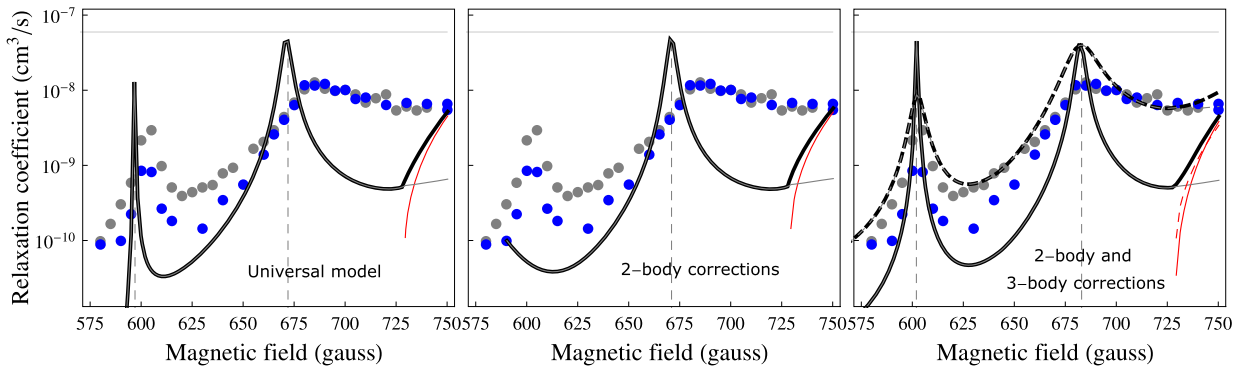

Fig. 6. Relaxation coefficient for dimer 23 colliding with atom 1 as a function of magnetic field. The grey and blue dots indicate the measurements from Refs. [7] and [6]. Left: universal model with $|\Lambda| = 1.165\bar{a}^{-1}$ and $\eta = 0.016$ – see similar calculations in Refs. [30,37]. Middle: contact model with $|\Lambda| = 1.455\bar{a}^{-1}$ and $\eta = 0.0033$. Right: contact model with the energy-dependent $|\Lambda|$ of Fig. 8 and $\eta = 0.0033$ (dashed curves: $\eta = 0.0400$). Black curves show the total relaxation coefficient, red curves show the relaxation to dimer 12, and grey curves show the relaxation to deep dimers. The horizontal line indicates the unitarity limit given by the typical collisional energy (~ 100 nK) in the experiments.

$E - E_{12} = \frac{3}{4}\frac{\hbar^2 Q_1^2}{m}$, the quantities $\tilde{\chi}_i$ can be written as:

$$\chi_i(P) = \sqrt{\mathcal{N}_i}\left(\delta_{i1}(2\pi)^3 \delta^3(\vec{P} - \vec{Q}_1) + \frac{4\pi f_i(P)}{P^2 - Q_i^2 - i\varepsilon}\right) \tag{27}$$

corresponding to an incident wave and outgoing waves of amplitude $f_i(Q_i)$ and momentum $Q_i = \sqrt{\frac{4}{3}(\frac{m}{\hbar^2}E + \kappa_i^2)}$. The relaxation coefficient $K_{\text{rel}}^{i \neq 1}$ to shallow dimers (jk) is then obtained by calculating the flux of the corresponding outgoing wave:

$$K_{\text{rel}}^i = \frac{4h}{m} Q_i |f_i(Q_i)|^2 \tag{28}$$

and the total relaxation coefficient is

$$K_{\text{rel}} = \frac{4h}{m}\left(\text{Im} f_1(Q_1) - Q_1 |f_1(Q_1)|^2\right) \tag{29}$$

Similarly to three-body recombination, whenever the magnetic field is close to the meeting point between a dimer and trimer, a resonance occurs which strongly enhances the relaxation coefficient. Indeed, two peaks were observed near the expected meeting points, at 602 G and 685 G [6,7] – see Fig. 6. However, the significant deviation of the second peak location from the expected value 672 G is somewhat surprising. Indeed, we checked that if we change the three-body parameter to obtain a peak at the measured 685 G, then the peak in the 3-recombination coefficient moves to 865 G, which seems incompatible with the measured value of 895 G in Ref. [3].

Similar measurements of the relaxation coefficient involving a dimer (12) colliding with atom 3 [7] revealed some dips in the relaxation coefficient at 610 G and 690 G – see Fig. 7. These dips are expected to result from two-pathway interferences
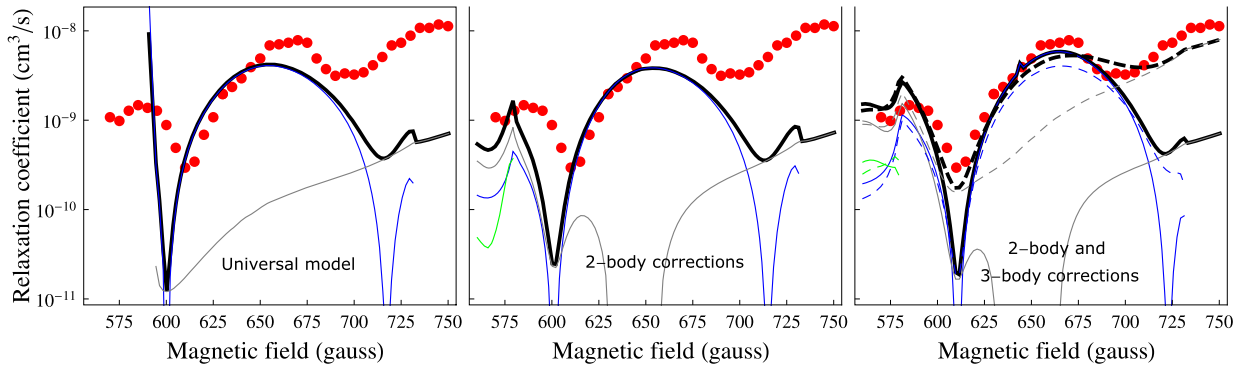
Fig. 7. Relaxation coefficient for dimer 12 colliding with atom 3 as a function of magnetic field. The red dots show the results of the measurements from Ref. [7]. The same conventions as in Fig. 6 are used.
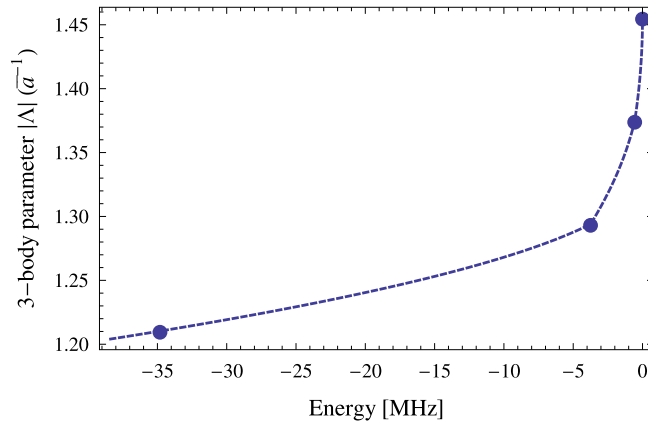

Fig. 8. Energy dependence of the three-body parameter Λ (in units of $\bar{a}^{-1}$) of the single-channel contact model adjusted to fit measured resonances. Each dot corresponds to an adjustment to a peak or dip of the relaxation coefficient.

related to the Efimov physics of the system [11]. Actually only the first dip appears as a clear signature of such interference. The second dip, as our calculations suggest, may be due to the combined effect of relaxation to shallow dimers and deep dimers. While both the universal and single-channel contact models predict a dip at 600 G, the real dip is again shifted away from the theoretical expectation.

Since all non-universal two-body corrections have been taken into account in the theoretical models, we concluded in Ref. [6] that a non-universal three-body correction is also needed. In the contact model, non-universal two-body corrections arise from the energy dependence of the scattering lengths $a_i(p)$. In the same fashion, we expect the three-body parameter Λ to be energy-dependent in general. By adjusting the value of $\Lambda(p)$ to fit each peak and dip locations we obtain some insight on this energy dependence. The result is plotted in Fig. 8 and looks consistent with a smooth but non-linear variation with energy. By interpolating $\Lambda(p)$ as a function of p, we can recalculate all previous curves and obtain reasonable agreement with experimental data, see Figs. 1, 6, and 7. This adjusted non-universal three-body model predicts that the ground-state Efimov trimer at large magnetic field is shifted by about 20 MHz from the universal prediction. Direct measurement of that energy would clearly validate or invalidate our assumption of the energy dependence of the three-body parameter Λ. The fact that the three-body parameter of an effective theory is energy-dependent to describe the ground-state trimer is not surprising, since ground states of Efimov series are always non-universal. It is less obvious, however, why it is also energy-dependent near the second trimer, which should be closer to universality.

4.2.2. Atom–dimer association spectroscopy

Very recently, the binding energy of the excited Efimov trimer was directly observed by association spectroscopy [15,27]. The experimentalists prepared a mixture of dimers and atoms, and applied a radio-frequency field to induce a transition to the trimer state. The preliminary results [15] reported excellent agreement with our own theoretical prediction [6] of the binding energy based on the single-channel contact model with the energy-dependent three-body parameter $\Lambda(p)$ – see Fig. 9. However, it turns out that the thermal shift of the association peaks is non-negligible in this experiment, and was not taken into account in the reported measurements of the binding energies. Correcting for these shifts makes the measurements deviate significantly from the original prediction. Worse still, to account for the deviation, the parameter
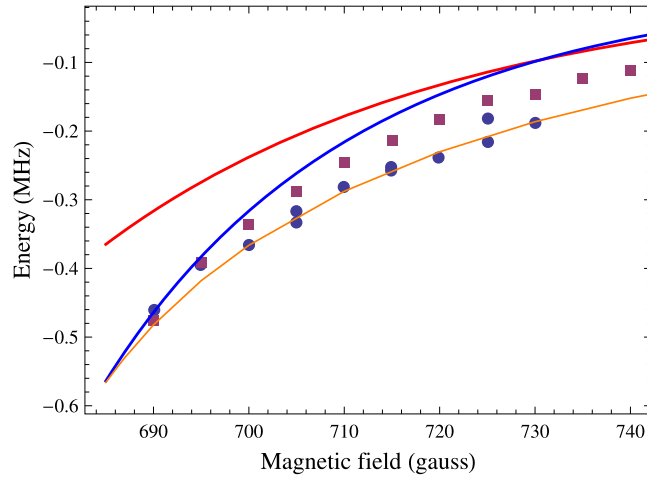
Fig. 9. Direct measurements of the second trimer energy: dots correspond to measurements of Ref. [15], which were taken at about 1 μK, and squares show the results of the measurements in Ref. [27] which were taken at lower temperature where thermal shifts are negligible. Using the same conventions as Fig. 1, thick curves represent the dimer energies and the orange curve represents the trimer energy obtained from the single-channel contact model with the energy-dependent three-body parameter shown in Fig. 8.

$\Lambda(p)$ should be adjusted in a way which breaks its expected smooth variation with energy. This problem is the subject of a separate study [27].

5. Conclusion

In this article we provided an overview of the various experimental results concerning the Efimov physics in a three-component lithium 6 system. Using different theoretical models, we found that the Efimov features measured at nearly zero energy are essentially consistent with the so-called Efimov scenario based on the universal theory developed in Vitaly Efimov's original papers. However, the features measured at negative energy, although qualitatively consistent with the Efimov scenario, show some significant deviations from universal theory, as well as theories which fully take into account non-universal two-body corrections. To account for this, we introduced phenomenological non-universal three-body corrections through an energy dependence of the three-body parameter adjusted the experimental data. While most measurements can be explained by this *ad hoc* parametrisation, it does not seem to be consistent with the very recent measurements of a trimer's binding energy, and further studies are needed to fully understand the physics at negative energy. The two-body model which the present study is based on is thought to be very accurate. However, even minor inaccuracies at the two-body level has been shown to be important in the three-body physics of other systems [38], and therefore deserve further investigation in our system as well.

Appendix A

Here, we give the derivation of Eq. (10). From Eq. (9), we perform the inverse Fourier transformation with respect to the second variable:

$$\tilde{\Psi}(\vec{P},\vec{r}) = \tilde{\Psi}_0(\vec{P},\vec{r}) + \left[\frac{e^{-\gamma_P|\vec{r}|}}{|\vec{r}|} \tilde{\chi}_1(\vec{P}) + 4\pi \int \frac{\tilde{\chi}_2(\vec{P}_2) + \tilde{\chi}_3(\vec{P}_3)}{\frac{3}{4}P^2 + p^2 - mE/\hbar^2 + i\varepsilon} e^{i\vec{p}\cdot\vec{r}} \frac{d^3\vec{p}}{(2\pi)^3} \right] \tag{30}$$

Then, applying the operator $\lim_{r\to 0} \frac{\partial}{\partial r}(r\cdot)$, and using the definition of $\tilde{\chi}_1$, we find:

$$-\frac{1}{a_1(i\gamma_P)} \tilde{\chi}_1(\vec{P}) = \left[\tilde{\Psi}_0(\vec{P},\vec{r}) \right]_{r\to 0} + \left[-\gamma_P \tilde{\chi}_1(\vec{P}) + 4\pi \int \frac{\tilde{\chi}_2(\vec{P}_2) + \tilde{\chi}_3(\vec{P}_3)}{\frac{3}{4}P^2 + p^2 - mE/\hbar^2 + i\varepsilon} \frac{d^3\vec{p}}{(2\pi)^3} \right] \tag{31}$$

Using $\vec{P}_2 = -\frac{\vec{P}}{2} - \vec{p}$, and $\vec{P}_3 = -\frac{\vec{P}}{2} + \vec{p}$, we can change the integration variable to get

$$-\frac{1}{a_1(i\gamma_P)} \tilde{\chi}_1(\vec{P}) = \left[\tilde{\Psi}_0(\vec{P},\vec{r}) \right]_{r\to 0} + \left[-\gamma_P \tilde{\chi}_1(\vec{P}) + 4\pi \int \frac{\tilde{\chi}_2(\vec{q}) + \tilde{\chi}_3(\vec{q})}{\frac{3}{4}P^2 + (\vec{q} + \frac{\vec{P}}{2})^2 - mE/\hbar^2 + i\varepsilon} \frac{d^3\vec{q}}{(2\pi)^3} \right] \tag{32}$$

$$\left(\gamma_P - \frac{1}{a_1(i\gamma_P)} \right) \tilde{\chi}_1(\vec{P}) - 4\pi \int \frac{\tilde{\chi}_2(\vec{q}) + \tilde{\chi}_3(\vec{q})}{P^2 + q^2 + \vec{P}\cdot\vec{q} - mE/\hbar^2 + i\varepsilon} \frac{d^3\vec{q}}{(2\pi)^3} = \left[\tilde{\Psi}_0(\vec{P},\vec{r}) \right]_{r\to 0} \tag{33}$$

Assuming that $\tilde{\chi}_i(\vec{q}) = \tilde{\chi}_i(q)$, and writing the integration element $d^3\vec{q} = q^2\, dq\, d\varphi\, d(-\cos\theta)$, with $\vec{P} \cdot \vec{q} = Pq\cos\theta$, we can perform the integration over the angles φ and θ:

$$\left(\gamma_P - \frac{1}{a_1(i\gamma_P)}\right)\tilde{\chi}_1(P)$$
$$-\frac{4\pi}{8\pi^3}\int\left(\int_0^{2\pi} d\varphi\right)\left(\int_{-1}^1 \frac{d(-\cos\theta)}{P^2 + q^2 - Pq\cos\theta - mE/\hbar^2 + i\varepsilon}\right)(\tilde{\chi}_2(q) + \tilde{\chi}_3(q))q^2\, dq = \left[\tilde{\Psi}_0(\vec{P},\vec{r})\right]_{r\to 0} \tag{34}$$

$$\left(-\frac{1}{a_1(i\gamma_P)} + \gamma_P\right)\tilde{\chi}_1(P) - \frac{1}{\pi}\int \frac{1}{Pq}\ln\frac{P^2 + q^2 + Pq - mE/\hbar^2}{P^2 + q^2 - Pq - mE/\hbar^2}(\tilde{\chi}_2(q) + \tilde{\chi}_3(q))q^2\, dq = \left[\tilde{\Psi}_0(\vec{P},\vec{r})\right]_{r\to 0} \tag{35}$$

from which we obtain Eq. (10) after introducing a cutoff Λ to the integral.

Appendix B

Here we derive the connection between the upper bound Λ of the integral in Eq. (10) and the boundary condition at short distance between the three particles. According to Danilov [20] and Minlos and Faddeev [39], the solutions $\tilde{\chi}_i(\vec{p})$ of the original Skorniakov–Ter-Martirosian equations (without upper bound Λ) are superpositions of two linearly independent solutions, which have the following asymptotic form:

$$\tilde{\chi}_i(\vec{p}) \underset{p\to\infty}{\to} A\frac{\sin(s_0\ln p)}{p^2} + B\frac{\cos(s_0\ln p)}{p^2} \propto \frac{\sin(s_0\ln\frac{p}{\Lambda_0})}{p^2} \tag{36}$$

where $s_0 \approx 1.00624$ is a constant. Thus, some extra condition can determine one particular solution (up to normalisation) by fixing the ratio $B/A = \tan(s_0\ln\Lambda_0)$. The quantity Λ_0 is the three-body parameter of the original Efimov theory. It is set by imposing a boundary condition on the wave function at short distance [1]. Alternatively, one can cut off the integral in Eq. (10) at some high momentum Λ [21,30,32], and this imposes the condition that the remaining part of the integral be zero:

$$\int_\Lambda^\infty dq\, \frac{q}{P}\ln\frac{P^2 + q^2 + Pq - mE/\hbar^2}{P^2 + q^2 - Pq - mE/\hbar^2}(\tilde{\chi}_j(q) + \tilde{\chi}_k(q)) \approx \int_\Lambda^\infty 4\frac{\sin(s_0\ln\frac{k}{\Lambda_0})}{k^2}\, dk = 0 \tag{37}$$

This condition selects a particular solution. By evaluating the above integral, one obtains

$$4\frac{s_0\cos(s_0\ln\frac{\Lambda}{\Lambda_0}) + \sin(s_0\ln\frac{\Lambda}{\Lambda_0})}{(\Lambda/\Lambda_0)(1 + s_0^2)} = 0 \tag{38}$$

which gives an explicit relation between the three-body parameter Λ_0 and the imposed cutoff Λ:

$$\Lambda_0 = \Lambda\exp\left(\frac{\arctan s_0 + \pi n}{s_0}\right), \quad \text{with } n \text{ integer.} \tag{39}$$

Appendix C

The expression for the total loss rate coefficient at zero energy, Eq. (25), can be seen as a consequence of the optical theorem. Here we indicate a short derivation. We start from the wave function in Eq. (9) in space coordinates at zero energy

$$\Psi(\vec{R},\vec{r}) = 1 + \sum_j \int \frac{d^3\vec{P}_j}{(2\pi)^3}\frac{d^3\vec{p}_j}{(2\pi)^3}\frac{4\pi}{\frac{3}{4}P_j^2 + p_j^2 + i\varepsilon}\tilde{\chi}_j(\vec{P}_j)e^{i\vec{P}_j\cdot\vec{R}_j}e^{i\vec{p}_j\cdot\vec{r}_j} \tag{40}$$

For large R_j, *i.e.* when all three atoms are far from each other, it can be approximated as $\Psi(\vec{R},\vec{r}) = 1 + G_0(\vec{R},\vec{r})\sum_j \tilde{\chi}_j(\vec{0})$, where

$$G_0(\vec{R},\vec{r}) = \int \frac{d^3\vec{P}_j}{(2\pi)^3}\frac{d^3\vec{p}_j}{(2\pi)^3}\frac{4\pi}{\frac{3}{4}P_j^2 + p_j^2 + i\varepsilon}e^{i\vec{P}_j\cdot\vec{R}_j}e^{i\vec{p}_j\cdot\vec{r}_j} = \frac{2\sqrt{3}}{(3\pi/2)^2}\frac{1}{\mathcal{R}^4} \tag{41}$$

and $\mathcal{R} = \sqrt{r^2 + \frac{4}{3}R^2}$ is the hyper-radius of the system. Calculating the flux of probability current of the wave function through a large hypersphere S, we obtain

$$\frac{2\hbar}{m}\mathrm{Im}\int_S \Psi^* \vec{\nabla}_{\mathcal{R}}\Psi \cdot d\vec{S} = \frac{2\hbar}{m}\left(\int_S \vec{\nabla}_{\mathcal{R}} G_0 \cdot d\vec{S}\right)\mathrm{Im}\sum_i \tilde{\chi}_i(0) \tag{42}$$

$$= \frac{2\hbar}{m}\left(\left(\frac{\sqrt{3}}{2}\right)^3 \frac{dG_0}{d\mathcal{R}}\frac{2\pi^3 \mathcal{R}^5}{\Gamma[3]}\right)\mathrm{Im}\sum_i \tilde{\chi}_i(0) \tag{43}$$

$$= -\frac{4h}{m}\mathrm{Im}\sum_i \tilde{\chi}_i(0) \tag{44}$$

This incoming flux should balance the outgoing fluxes in other sectors where two atoms are recombined into a shallow dimer [Eq. (23)], as well as the loss induced by the imaginary part of the three-body parameter Λ, which phenomenologically describes recombination to deep dimers. Therefore, Eq. (44) represents the total recombination coefficient K_{rec}.

References

[1] V.N. Efimov, Sov. J. Nucl. Phys. 12 (1970) 589;
    V. Efimov, Nucl. Phys. A 210 (1973) 157.
[2] F. Ferlaino, R. Grimm, Physics 3 (2010) 9.
[3] J.R. Williams, E.L. Hazlett, J.H. Huckans, R.W. Stites, Y. Zhang, K.M. O'Hara, Phys. Rev. Lett. 103 (2009) 130404.
[4] M. Zaccanti, B. Deissler, C. D'Errico, M. Fattori, M. Jona-Lasinio, S. Müller, G. Roati, M. Inguscio, G. Modugno, Nat. Phys. 5 (2009) 586–591.
[5] G. Barontini, et al., Phys. Rev. Lett. 103 (2009) 043201.
[6] S. Nakajima, M. Horikoshi, T. Mukaiyama, P. Naidon, M. Ueda, Phys. Rev. Lett. 105 (2010) 023201.
[7] T. Lompe, T.B. Ottenstein, F. Serwane, K. Viering, A.N. Wenz, G. Zürn, S. Jochim, Phys. Rev. Lett. 105 (2010) 103201.
[8] N. Gross, Z. Shotan, S. Kokkelmans, L. Khaykovich, Phys. Rev. Lett. 103 (2009) 163202.
[9] S.E. Pollack, D. Dries, R.G. Hulet, Science 326 (2009) 1683.
[10] C. Chin, R. Grimm, P. Julienne, E. Tiesinga, Rev. Mod. Phys. 82 (2010) 1225.
[11] J.P. D'Incao, B.D. Esry, Phys. Rev. Lett. 103 (2009) 083202.
[12] J.H. Huckans, et al., Phys. Rev. Lett. 102 (2009) 165302.
[13] T.B. Ottenstein, T. Lompe, M. Kohnen, A.N. Wenz, S. Jochim, Phys. Rev. Lett. 101 (2008) 203202.
[14] S. Knoop, F. Ferlaino, M. Berninger, M. Mark, H.-C. Nägerl, R. Grimm, J.P. D'Incao, B.D. Esry, Phys. Rev. Lett. 104 (2010) 053201.
[15] T. Lompe, T.B. Ottenstein, F. Serwane, A.N. Wenz, G. Zürn, S. Jochim, Science 330 (2010) 940.
[16] M. Bartenstein, et al., Phys. Rev. Lett. 92 (2004) 120401.
[17] E. Braaten, H.-W. Hammer, Ann. Phys. 322 (2007) 120–163.
[18] D.S. Petrov, Phys. Rev. Lett. 93 (2004) 143201.
[19] G.V. Skorniakov, K.A. Ter-Martirosian, Sov. Phys. JETP 4 (1957) 648.
[20] G.S. Danilov, JETP 40 (1961) 498, Sov. Phys. JETP 13 (1961) 349.
[21] V.F. Kharchenko, Yad. Fiz. 16 (1972) 310–315, Sov. J. Nucl. Phys. 16 (1972) 173.
[22] V. Efimov, Phys. Rev. C 44 (1991) 2303.
[23] M.D. Lee, T. Köhler, P.S. Julienne, Phys. Rev. A 76 (2007) 012720.
[24] M. Jona-Lasinio, L. Pricoupenko, Phys. Rev. Lett. 104 (2010) 023201.
[25] M. Jona-Lasinio, L. Pricoupenko, Y. Castin, Phys. Rev. A 77 (2008) 043611.
[26] F. Werner, L. Tarruell, Y. Castin, Eur. Phys. J. B 68 (2009) 401.
[27] S. Nakajima, M. Horikoshi, T. Mukaiyama, P. Naidon, M. Ueda, arXiv:1010.1954, 2010.
[28] D.S. Petrov, C. Salomon, G.V. Shlyapnikov, Phys. Rev. Lett. 93 (2004) 090404;
    D.S. Petrov, C. Salomon, G.V. Shlyapnikov, Phys. Rev. A 71 (2005) 012708.
[29] F. Werner, Y. Castin, Phys. Rev. Lett. 97 (2006) 150401.
[30] E. Braaten, H.-W. Hammer, D. Kang, L. Platter, Phys. Rev. A 81 (2010) 013605.
[31] J.P. D'Incao, C.H. Greene, B.D. Esry, J. Phys. B: At. Mol. Opt. Phys. 42 (2009) 044016.
[32] E. Braaten, H.-W. Hammer, D. Kang, L. Platter, Phys. Rev. Lett. 103 (2009) 073202.
[33] P. Naidon, M. Ueda, Phys. Rev. Lett. 103 (2009) 073203.
[34] S. Floerchinger, R. Schmidt, C. Wetterich, Phys. Rev. A 79 (2009) 053633.
[35] A.N. Wenz, T. Lompe, T.B. Ottenstein, F. Serwane, G. Zürn, S. Jochim, Phys. Rev. A 80 (2009) 040702.
[36] S.T. Rittenhouse, Phys. Rev. A 81 (2010) 040701.
[37] H.-W. Hammer, D. Kang, L. Platter, Phys. Rev. A 82 (2010) 022715.
[38] N. Gross, Z. Shotan, S. Kokkelmans, L. Khaykovich, Phys. Rev. Lett. 105 (2010) 103203.
[39] R.A. Minlos, L.D. Faddeev, JETP 41 (1961) 1850.